ELSEVIER

Journal of Nuclear Materials 241–243 (1997) 946–949

journal of nuclear materials

Boundary modelling of the stellarator Wendelstein 7-X

H. Renner *, E. Strumberger, J. Kisslinger, J. Nührenberg, H. Wobig

Max-Planck-Institut für Plasmaphysik, EURATOM-Ass. IPP, Boltzmannstr. 2, D-85748 Garching, Germany

Abstract

To justify the design of the divertor plates in W7-X the magnetic fields of finite-β HELIAS equilibria for the so-called high-mirror case have been computed for various average β-values up to $\langle \beta \rangle = 0.04$ with the NEMEC free-boundary equilibrium code [S.P. Hirshman, W.I. van Rij and W.I. Merkel, Comput. Phys. Commun. 43 (1986) 143] in combination with the newly developed MFBE (magnetic field solver for finite-beta equilibria) code. In a second study the unloading of the target plates by radiation was investigated. The B2 code [B.J. Braams, Ph.D. Thesis, Rijksuniversiteit Utrecht (1986)] was applied for the first time to stellarators to provide of a self-consistent modelling of the SOL including effects of neutrals and impurities.

Keywords: W7-X; Helical divertor; Boundary MHD; 2D model; Fluid simulation

1. Introduction

For the new HELIAS [1] stellarator W7-X (major radius $R = 5.5$ m, plasma radius $a = 0.55$ m, magnetic field of $B = 3$ T produced by a superconducting modular coil system), a divertor concept for stationary operation with a power deposition of up to 10 MW has been developed. An attribute of the selected magnetic configuration is an inherent divertor with the LCMS (last closed magnetic surface) of the confinement region being either defined by the inner separatrix of islands (being intersected by target plates) or by an ergodised boundary with remnants of islands. An open divertor system [2] has been designed to achieve effective power and particle exhaust in the wide magnetic parameter range. The optimisation of the geometry of the divertor (target and baffle plates) was based on field line tracing for the vacuum configurations and simulation of perpendicular transport by 'field line diffusion' (Monte-Carlo code) to calculate the power deposition on the targets, whereas the pumping efficiency was estimated by means of the EIRENE [3] code taking into account reasonable boundary parameters. Local power densities up to 8 MW/m^2 at the target plates were obtained for a wide range of magnetic parameters for the worst case at low-density and high-temperature operation.

2. SOL modelling at W7-X

2.1. Magnetic fields and SOL of finite-β equilibria

The high-mirror vacuum magnetic field of W7-X and the corresponding magnetic fields of finite-β equilibria have been calculated on a grid which contains the plasma and the entire scrape-off layer region with divertor and baffle plates. While the vacuum magnetic field can be easily obtained from the external coils using Biot–Savart's law, for the computation of finite-β magnetic fields a new code, MFBE [4], was developed, which evaluates these magnetic fields by using the results of the NEMEC free-boundary finite-β equilibrium code [5]. Here the resulting magnetic field for $\langle \beta \rangle = 0.04$ is compared with the corresponding vacuum field. The sufficiently small shift of the magnetic surfaces and the small change of the rotational transform with increasing β are important properties of the optimised W7-X. These properties are the basic requirements to guarantee that the target and baffle plate configuration works without geometrical adjustments for various finite-β equilibria. Fig. 1 shows the magnetic field structures of the vacuum case and $\langle \beta \rangle = 0.04$ at the

* Corresponding author. Tel.: +49-89 3299 1417; fax: +49-89 3299 2579; e-mail: hermann.renner@ipp-garching.mpg.de.

PII S0022-3115(96)00637-X

bean-shaped cross-section, which serves as a representative example of the various cross-sections. In both cases the divertor plates intersect the macroscopic 'islands' because the fixed points of the 5/5 islands hardly change their positions. The plasma boundaries of the finite-β equilibria lie inside the LCMS of the vacuum field, while the edge region ergodizes and the width of the 5/5 islands extends with increasing β.

These slight variations of the magnetic field structure lead to an increasing distance between LCMS and divertor plates, which is a desirable effect. The long ($L > 200$ m) and intermediate ($L = 45$–200 m) field lines come close to the LCMS so that most of the power and particles flow along them to the divertor plates. The wetted areas of these SOL field lines and their corresponding intersection angles are decisive for the power load on the plates. A comparison of the interaction of the flux bundles with the target surfaces (Fig. 2) shows that the wetted areas formed by long and intermediate field lines increase with increasing β, because of the increasing ergodization of the edge region and the increasing island width. While in the case of the vacuum magnetic field only the divertor plates localised at the radially inner side of the plasma column are intersected by long and intermediate field lines, in the case of $\langle \beta \rangle = 0.04$ large areas including all target plates are intersected by these field lines because of the slight outward shift of the magnetic surfaces. The intersection angles on the divertor plates (typical values are 0–3°) differ only slightly from those of the vacuum case (the maximum difference is $\pm 0.2°$). The total size of the wetted area for the long field lines ($L > 45$ m) is $A = 1.9$ m^2 at the vacuum case and $A = 5$ m^2 at $\langle \beta \rangle = 4\%$. Simulation of the energy transport across the field lines by 'diffusion' of field lines leads to a further increase of these intersection areas.

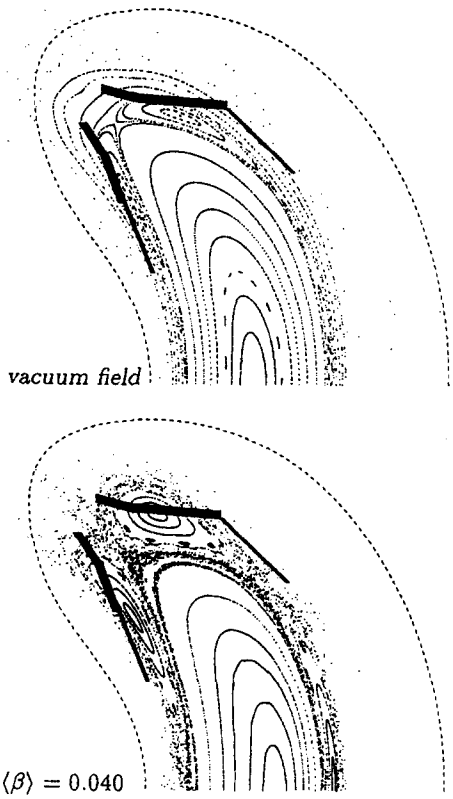

Fig. 1. Poincaré plot of the upper half of the symmetric bean-shaped cross-section for the vacuum case and $\langle \beta \rangle = 0.04$. The thick bars show the target plates, whereas the thin ones mark the baffle plates.

2.2. Simulation of the W7-X edge plasma using the B2-code

The multi-fluid code B2 [6] has been adapted to describe the SOL parameters. The code is based on a rectangular grid which is generated approximately for W7-X [7]. The island divertor concept makes benefit of the large islands in the boundary region at rational values of the rotational transform, e.g. 5/5 in W7-X. Due to the five-fold symmetry it is sufficient to restrict the calculations to one island region equal to a sector of 1/5 of the poloidal circumference. Since B2 is a 2D-code, the geometry of the plasma edge must be averaged (distances) or integrated (areas and volume) in the toroidal direction. Fig. 3 shows the averaged island geometry used in our calculations. The target plates intersect the islands and the private flux region. The bottom boundary of the grid is connected with the core plasma. The left and right sides are connected with the neighbouring islands and are simulated in the calculations by symmetry planes.

The plasma density and the power flux (2 MW per island) are prescribed at the border to the main plasma in the radial direction. The cross-field thermal diffusivity for electrons and ions is taken to be 1 m^2/s, the value of the particle diffusivity is 0.5 m^2/s [7]. The present study is made with a simple neutral particle recycling model using recycling coefficients at the wall of 1 and at the targets of 0.98 (particle exhaust by pumping). Fig. 4 presents the boundary plasma parameters at the target plate versus the radial cell number (see Fig. 3). In the case with the low separatrix mid-plane density rather high temperatures and a low density at the target are obtained. With increasing mid-plane density, a steep decrease of the temperature at the targets and a drastic increase of the density occur. For a mid-plane density of 2.5×10^{19} m^{-3} the density at the target is about 5 times higher than at the separatrix and is increasing still further towards the 0-point of the island, thus showing that the high recycling regime is already attainable at a moderate density. The power densities representing averaged values along the wetted length of the target plates are shown for the three densities also.

In the second part of this study, the impurity transport and radiation losses of carbon with a prescribed concentra-

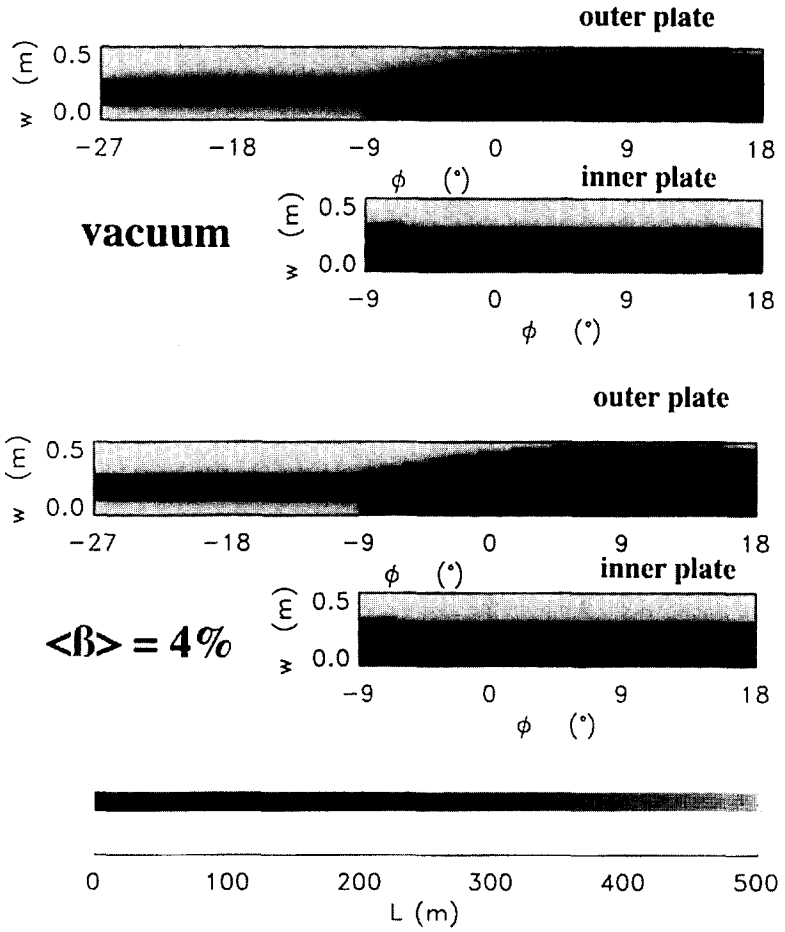

Fig. 2. Plasma facing surfaces of one divertor unit for the case vacuum field and $\beta = 4\%$ equilibrium. The interaction pattern as result of the calculation are characterised on the outer and inner plate. w describes the poloidal width, θ is the toroidal angle, $\theta = 0°$ represents the symmetry plane where the plasma cross-section is bean-shaped. The field line foot prints are ordered according to their field line length.

tion of 1.7% at the separatrix mid-plane and a recycling factor for carbon of 1 everywhere is taken into account in a simplified approach not dealing with the production process. The electron density is set to 3.1×10^{19} m^{-3} at the separatrix mid plane. The radiated power resulting from carbon is 350 kW, concentrated in front of the target

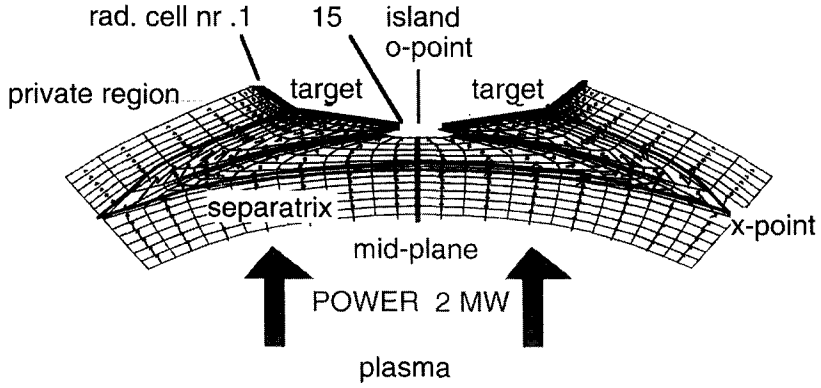

Fig. 3. Geometry of one island sector as being averaged in toroidal direction. The left and right sides of the sector are connected with the neighbouring islands. The arrows show the calculated power flow.

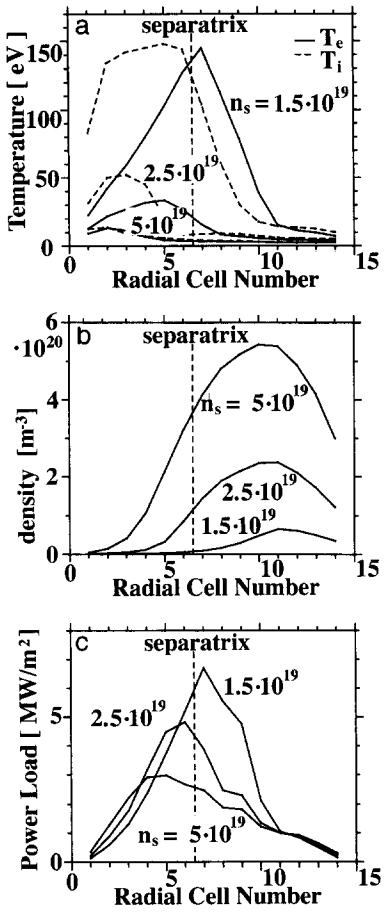

Fig. 4. Temperature, density and power load versus the radial cell number. The varying parameter is the separatrix density n_s at the mid-plane. The total power flow across the separatrix is 10 MW.

plates. There, the maximum power density at the targets is reduced by about 25% compared to the case without carbon. The plasma density increases and the electron temperature drops.

3. Conclusion

The magnetic structures of finite-β equilibria differ only slightly from the corresponding vacuum field. The edge region ergodizes and the width of the macroscopic islands increases with increasing β, while the O- and X-points of these islands hardly change their positions. Due to this behaviour the island divertor designed for the vacuum field works for finite-β equilibria also. As in the vacuum case there are no leading edges and the interaction of charged particles leaving the plasma is completely removed from the vessel wall. The variation of the intersection angles with increasing β is not significant, while the intersection areas of the long field lines and the distances along the field lines from the divertor plates to the LCMS even increase.

Although only a 3D study can lead to a completely satisfying description of the boundary, the first attempt of a self-consistent modelling on the basis of the adapted B2 code can already demonstrate a significant unloading of the target plates by achieving a high recycling mode at moderate separatrix densities above 2×10^{19} m^{-3}. Taking into account reasonable impurity concentrations on the order of 1% C, a further reduction of the electron temperature and the power deposition to the target plates is found with radiation concentrated in front of the target plates.

References

[1] J. Nührenberg and R. Zille, Phys. Lett. A 114, 129.
[2] H. Greuner et al. Proc. 18th SOFT, Karlsruhe, Vol. 1 (1994) p. 323.
[3] D. Reiter, Jülich Report 1947, Jülich (1984).
[4] E. Strumberger, Nucl. Fusion 36 (1996) 891.
[5] S.P. Hirshman, W.I. van Rij and W.I. Merkel, Comput. Phys. Commun. 43 (1986) 143.
[6] B.J. Braams, Ph.D. Thesis, Rijksuniversiteit Utrecht (1986).
[7] J. Kisslinger et al., 22nd EPS, Bournemouth, Vol 19C-III (1995) p. 149.